International Journal of Solids and Structures 48 (2011) 1011–1023

Contents lists available at ScienceDirect

International Journal of Solids and Structures

journal homepage: www.elsevier.com/locate/ijsolstr

Mathematical programming approaches for the safety assessment of semirigid elastoplastic frames

S. Tangaramvong *, F. Tin-Loi

School of Civil and Environmental Engineering, The University of New South Wales, Sydney, NSW 2052, Australia

ARTICLE INFO

Article history:
Received 23 September 2010
Received in revised form 30 November 2010
Available online 13 December 2010

Keywords:
Complementarity
Elastoplastic analysis
Limit analysis
Mathematical programming
Safety assessment
Semirigid connections

ABSTRACT

This paper presents two complementary mathematical programming based approaches for the accurate safety assessment of semirigid elastoplastic frames under quasistatic loads. The inelastic behavior of the flexible connections and material plasticity are accommodated through piecewise linearized nonlinear yield surfaces. As is necessary for this class of structures, geometric nonlinearity is taken into account. Moreover, only a 2nd-order geometric approximation is included as this is sufficiently accurate for practical structures. The work described has a twofold contribution. First, we develop an algorithm that can robustly and efficiently process the complete (path-dependent) nonholonomic response of the structure in a stepwise (path-independent) holonomic fashion. The governing formulation is cast in mixed static-kinematic variables and leads naturally to what is known in the mathematical programming literature as a mixed complementarity problem (MCP). The novelty of the proposed algorithm is that it processes the MCP directly without using some iterative (and often cumbersome) predictor–corrector procedure. Second, in the spirit of simplified analyses, the classical limit analysis approach is extended to compute the limit load multiplier under the simultaneous influence of joint flexibility, material and geometric nonlinearities, and limited ductility. Our formulation is an instance of the challenging class of optimization problems known as a mathematical program with equilibrium constraints (MPEC). Various nonlinear programming based algorithms are proposed to solve the MPEC. Finally, four numerical examples, concerning practical structures and benchmark cases, are provided to illustrate application of the analyses as well as to validate the accuracy and robustness of the proposed schemes.

1. Introduction

Steel frames with flexible connections represent a common class of structures for which it is important to assess reliably and efficiently their structural safety. With the rapid advancement of computer technology and the ever increasing utilization of limit state principles, the 2nd-order inelastic analysis of such semirigid elastoplastic structures has received considerable attention (see, e.g. Chen and Zhou, 1987; Lui and Chen, 1988; Anderson and Kavianpour, 1991; Tin-Loi and Misa, 1996).

The focus to date has primarily been on evolutive (step-by-step) analysis to trace the entire displacement response of the structure under a known applied loading regime. The methods used typically rely on some iterative technique, often based on primarily repeated elastic iterates. Such schemes are generally computational expensive, especially when practical large size structures are involved. It is often the case that very small load steps are required to achieve not only convergence but also an accurate solution to the underlying nonlinear problem.

The present work similarly targets the evolutive elastoplastic analyses of semirigid frames under quasistatic loads and a 2nd-order geometric assumption. Moreover, we also propose an extension of the classical limit analysis approach to compute, in a single step, the maximum load that the structure can sustain under the simultaneous influence of joint flexibility, material and geometric nonlinearities, and limited ductility. For these two types of analyses, we develop novel, efficient and robust techniques within a mathematical programming framework. The underlying mathematical structure in both our evolutive and extended limit analysis formulations is in fact a complementarity system (Maier, 1970, 1971). Complementarity defines the typical componentwise condition $w_j \dot{z}_j = 0$, $w_j \geqslant 0$ and $\dot{z}_j \geqslant 0$ for all j. Physically, it represents conditions that describe, for instance, plastic conformity. It is also pertinent to mention that such approaches are in fact quite generic and can be applied, obviously with some formal complications, to more sophisticated finite element models.

The novelty of our step-by-step analysis lies in the fact that it does not require the use of some expensive iterative predictor–

* Corresponding author. Tel.: +61 2 9385 5474; fax: +61 2 9385 6139.
E-mail address: sawekchai@unsw.edu.au (S. Tangaramvong).

0020-7683/$ - see front matter © 2010 Elsevier Ltd. All rights reserved.
doi:10.1016/j.ijsolstr.2010.12.003

corrector algorithm, as is often used (see, e.g. Forde and Stiemer, 1987; Comi and Maier, 1990; Tin-Loi and Misa, 1996; Tangaramvong and Tin-Loi, 2010b). Even in the presence of 2nd-order geometry, our approach can trace efficiently and accurately the complete (path-dependent) nonholonomic responses of practical (often large size) semirigid structures. The genesis of the scheme lies in the formulation and direct solution of the governing relations, cast as a special case of a mathematical programming problem known as a mixed complementarity problem or MCP (Dirkse and Ferris, 1995a). For efficiency and without loss of accuracy, we conveniently replace, as is often done, the exact nonholonomic rate problem by its finite incremental counterpart (Franchi et al., 1981). A special enumerative scheme (Tin-Loi et al., 2007) is incorporated in the algorithm so that such crucial physical instabilizing phenomena as bifurcation, snapback and post collapse responses can be identified.

As mentioned, we also propose a single step analysis aimed at calculating the maximum load capacity of the structure. Such types of "direct" or "simplified" analyses, the most well-known of which is the classical limit or shakedown analysis, are extremely valuable in a large number of practical engineering situations. They avoid expensive evolutive analyses, and represent a useful, competitive and increasingly appealing alternative (Chen, 2000). Due to the fact that the upper and lower bound theorems underpinning classical limit analysis are strictly only applicable to structures that satisfy some rather restrictive requirements (e.g. perfect plasticity, sufficient ductility and geometric linearity), we propose an extension. The original ideas and some applications of this approach that can simultaneously provide critical load and associated deformation information have been described recently (see, e.g. Tin-Loi et al., 2007; Ardito et al., 2008; Tangaramvong and Tin-Loi, 2009b, 2010a) . Similar to these works, we formulate the problem as a challenging instance of a nonconvex and nonsmooth optimization problem known as a mathematical program with equilibrium constraints or MPEC (Luo et al., 1996). These equilibrium constraints are more precisely, in our case, complementarity constraints and represent the main source of difficulty in solving MPECs. The novelty in this aspect of our present work lies in the solution algorithm: we process the MPEC directly, without the use of some outer level iterative procedures required when geometric effects are present (see, e.g. Tangaramvong and Tin-Loi, 2009b).

The present paper is organized as follows: Section 2 provides all the basic ingredients, namely statics, kinematics and constitutive laws, required to formulate the state problems in mixed static and kinematic variables for both nonholonomic and holonomic elastoplastic analyses of semirigid frames. Piecewise linearization of the nonlinear yield surface (Maier, 1970) is adopted. In Section 3, we develop the stepwise holonomic analysis formulation and describe the mathematical programming based numerical algorithm used to process, in a finite step fashion, the complete structural response. Section 4 formulates the extended limit analysis as an MPEC. Some difficulties in solving the MPEC are mentioned before we briefly describe three nonlinear programming (NLP) based approaches that may be suitable for its solution. Four numerical examples of practical structures are given, in Section 5, to illustrate application of the developed schemes. These examples serve not only to validate the accuracy of the analyses through benchmark results but also to illustrate the robustness and efficiency of the proposed stepwise holonomic and extended limit analysis algorithms. Finally, we conclude with some pertinent remarks in Section 6.

A word regarding notation is in order. Vectors and matrices are indicated in bold. A real vector $\mathbf{x}$ of size m is indicated by $\mathbf{x} \in \Re^m$ and a real $m \times n$ matrix $\mathbf{A}$ by $\mathbf{A} \in \Re^{m\times n}$. For brevity, a vector of functions $\mathbf{f}(\mathbf{x}) : \Re^m \to \Re^n$ is written simply as $\mathbf{f} \in \Re^n$.

2. Generic finite element model and governing relations

2.1. Discrete structural model

We assume that the structure under consideration has been discretized as an aggregate of finite elements. In this study, the material behavior is directly reflected by the element behavior, since the class of finite elements expressed in intrinsic, natural (in Prager's generalized sense) variables is adopted (Maier, 1970). This implies that the scalar product of generalized stress and strain vectors represents virtual work in the element concerned and is invariant with respect to rigid body motion. The stress resultant or generalized stress is obtained by integrating the assumed stress field across the section. Similarly, the associated strain resultant is computed by a suitable kinematic assumption associating each physical component of strains with displacements in global coordinates.

We adopt a conventional lumped plasticity model within a "line" finite element framework (see, e.g. Bolzon and Corigliano, 1997; Cocchetti and Maier, 2003; Tangaramvong and Tin-Loi, 2010a). This is eminently suitable since plastic strains will localize strongly in a limited number of fixed critical zones, whilst the remaining part of the structure can be considered to be still in the elastic regime. The model for this kind of structural behavior then involves a special instance of the class of discrete formulations consisting of an elastic solid with embedded interfaces or loci of possible displacement discontinuities. The displacement discontinuities incorporate the localized dissipative effects observed in the failures of the material in the large-scale problem, without the need to introduce explicitly the small scales (Ehrlich and Armero, 2005; Armero and Ehrlich, 2006). In addition to plastic hinges, this generic representation (Bolzon and Corigliano, 1997) can be used to describe decohesion and quasibrittle fracture processes, through interface laws which relate tractions to displacement jumps.

For the generic self equilibrated 2-D frame element i in Fig. 1, the generalized stress vector $\mathbf{s}^i \in \Re^3$ contains the three (independent) two end moments (s_2^i, s_3^i) and one axial force (s_1^i). The corresponding generalized strain vector $\mathbf{q}^i \in \Re^3$ consists of the corresponding end rotations (q_2^i, q_3^i) and axial deformation (q_1^i), which are explicitly taken as summation products of the generalized elastic strain vector $\mathbf{e}^i \in \Re^3$ and the generalized plastic strain vector $\mathbf{p}^i \in \Re^3$. Generalized plastic hinges are assumed to be confined at the member ends so that the material in between remains elastic.

To model a semirigid beam-to-column connection, a rotation spring with the nonlinear moment-relative rotation relationship shown in Fig. 2 is attached to the corresponding beam end (Chen and Zhou, 1987; Lui and Chen, 1988). This nonlinear moment–rotation curve (dashed line) of the spring element is approximately represented by the multilinear (solid lines) model. The flexible joint is modeled as a zero-length spring element, and a plastic

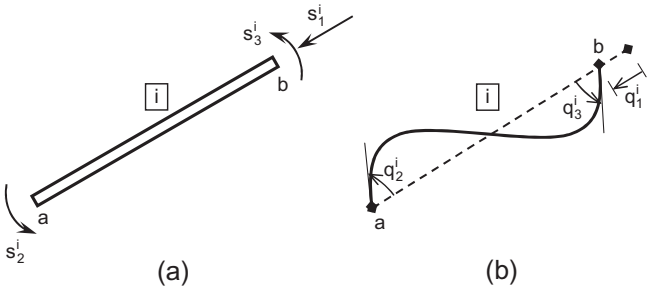

Fig. 1. Generic 2-D frame element i: (a) generalized stresses and (b) generalized st rains.

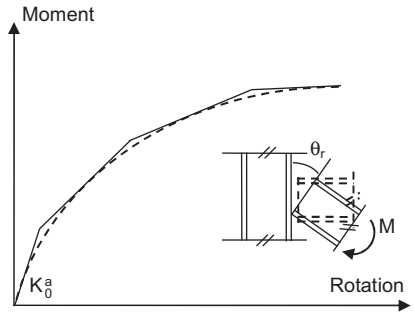

Fig. 2. Typical multilinear moment–rotation model of semirigid connections.

hinge is placed at the member end to respond to any inelastic deformation. In effect this model is an elastoplastic hinge that can simulate not only the initial elastic stiffness of the connection semirigidity but also its plastic behavior through the class of interacting piecewise linear laws (Maier, 1970).

The external loads, defined by a single load multiplier α, are assumed to be applied to the nodes. Distributed loads are simulated as equivalent concentrated forces on an appropriate number of nodes. The unconstrained nodal forces $\mathbf{F}^i$, defined with respect to a global reference axis system, are then expressed in terms of the load multiplier α, the given basic nodal load vector $\mathbf{f}^i$ and the fixed nodal load vector $\mathbf{f}_d^i$ as $\mathbf{F}^i = \alpha\mathbf{f}^i + \mathbf{f}_d^i$.

2.2. Governing elastoplastic formulations

In the section, we recall the two discrete mathematical programming formulations for classical evolutive elastoplastic analysis (Maier, 1970) of semirigid structures, for which piecewise linear approximations of nonlinear yield surfaces (see, e.g. Maier, 1970; Cocchetti and Maier, 2003; Tangaramvong and Tin-Loi, 2009a) have been adopted.

The first model, in the spirit of the flow theory of plasticity, assumes nonholonomy or path-dependence. This assumption correctly describes elastic unloading–reloading events, as is illustrated in the $s_2^i - q_2^i$ diagram of Fig. 3a, where any unloading from the horizontal branch of the moment–rotation law is elastic thus preserving the value of the previous plastic rotations; s_{2u} defines the yield capacity.

The second model deals with the approximate holonomic (path-independent) behavior in accordance with the deformation theory of plasticity. With reference to Fig. 3b, elastic unloading from the perfectly plastic branch is thus not permitted. The stress point is instead restricted to move in a reversible manner along the actual, original branch.

To account for geometric nonlinearity, the well-known simplified 2nd-order theory is adopted (see, e.g. Maier, 1971; Bolzon and Tin-Loi, 1999) in which up to only the 1st-power quantities of the exact geometrically nonlinear formulation are retained. This degree of geometric nonlinearity, as shown in our previous work (Tangaramvong and Tin-Loi, 2010b), is sufficiently accurate to predict the realistic behavior of practical frames. It is further assumed that displacements from the undeformed state are geometrically small.

The equilibrium condition for each elastic member i in the deformed state can be established by using the familiar geometric stiffness matrix $\mathbf{K}_G^i$ (Przemieniecki, 1985) which accounts for change of configuration with loading.

For a generic frame element i, the 2nd-order geometric nonlinearity can be conveniently described by introducing an additional (fictitious) transverse force π_f^i with corresponding displacement δ_f^i (De Freitas and Lloyd Smith, 1984-1985), as shown in Fig. 4. Clearly, the force π_f^i and the displacement δ_f^i represent the configuration change of the member.

Formulations for both nonholonomic and holonomic state models are achieved by simply manipulating the three appropriate basic ingredients, namely statics, kinematics and constitution, describing the intrinsic structural response.

2.2.1. Nonholonomic state problem

In terms of standard notation and well-known descriptions (e.g. Maier, 1970; Tangaramvong and Tin-Loi, 2010b), the governing nonholonomic relations for the whole structural system suitably discretized into n elements, d degrees of freedom, m natural generalized stresses (or strains) and y plastic yield conditions can be written as follows:

$$\alpha\mathbf{f} + \mathbf{f}_d = \mathbf{C}_0^{\mathrm{T}}\mathbf{s} + \mathbf{C}_f^{\mathrm{T}}\boldsymbol{\pi}_f, \tag{1}$$

$$\mathbf{q} = \mathbf{C}_0\mathbf{u}, \tag{2}$$

$$\boldsymbol{\delta}_f = \mathbf{C}_f\mathbf{u}, \tag{3}$$

$$\mathbf{q} = \mathbf{e} + \mathbf{p}, \tag{4}$$

$$\mathbf{s} = \mathbf{S}(\mathbf{s})\mathbf{e}, \tag{5}$$

$$\boldsymbol{\pi}_f = \mathbf{S}_f(\mathbf{s})\boldsymbol{\delta}_f, \tag{6}$$

$$\dot{\mathbf{p}} = \mathbf{N}\dot{\boldsymbol{\lambda}}, \tag{7}$$

$$\mathbf{w} = -\mathbf{N}^{\mathrm{T}}\mathbf{s} + \mathbf{H}\mathbf{z} + \mathbf{r} \geqslant \mathbf{0}, \quad \dot{\boldsymbol{\lambda}} \geqslant \mathbf{0}, \quad \mathbf{w}^{\mathrm{T}}\dot{\boldsymbol{\lambda}} = 0. \tag{8}$$

Equilibrium between forces $\alpha\mathbf{f} + \mathbf{f}_d \in \Re^d$ and the stress components (namely $\mathbf{s} \in \Re^m$ and $\boldsymbol{\pi}_f \in \Re^n$) is expressed by (1), where $\mathbf{C}_0 \in \Re^{m\times d}$ is the compatibility matrix and $\mathbf{C}_f \in \Re^{n\times d}$ the associated auxiliary compatibility matrix. For the sake of completeness, the explicit expressions of the two matrices $\mathbf{C}_0$ and $\mathbf{C}_f$ are provided in Appendix A. The linear compatibility condition given in (2) relating strains $\mathbf{q} \in \Re^m$ with nodal displacements $\mathbf{u} \in \Re^d$ applies, provided that additional displacements $\boldsymbol{\delta}_f \in \Re^n$, linearly proportional to the nodal displacements $\mathbf{u}$, are introduced in (3). The Lagrangian static-kinematic descriptions, as stated in (1)–(3), are thus de-

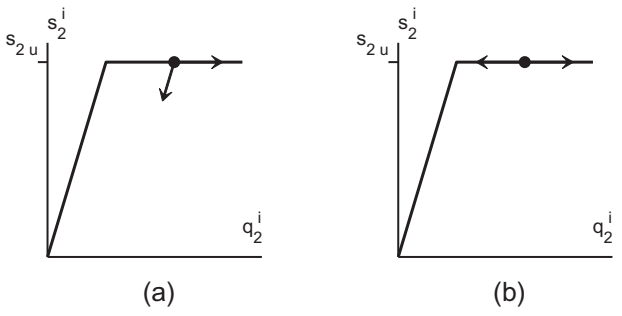

Fig. 3. Generic moment–rotation elastoplastic law: (a) nonholonomic and (b) holonomic.

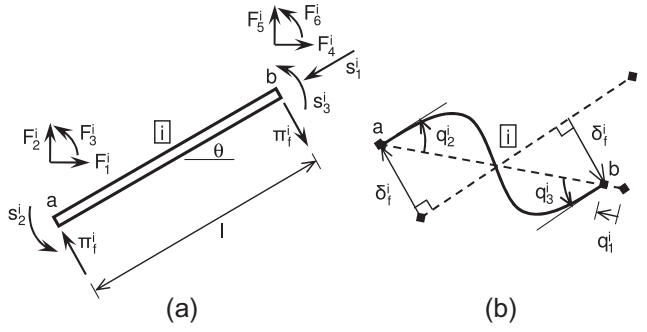

Fig. 4. Generic 2-D frame element i with 2nd-order geometric nonlinearity: (a) stresses and (b) strains.

scribed in the undeformed framework so that the duality relationship between equilibrium and compatibility of the structural system is preserved.

Relations (4)–(8) embody the nonholonomic elastoplastic constitutive laws. The additivity of elastic $\mathbf{e} \in \Re^m$ and plastic $\mathbf{p} \in \Re^m$ strains is given by (4). The elastic behavior is described in two parts: the relation (5) between stresses $\mathbf{s}$ and elastic strains $\mathbf{e}$, and (6) between fictitious forces $\boldsymbol{\pi}_f$ and corresponding deformations $\boldsymbol{\delta}_f$. The influence of both 2nd-order geometry and the initial elastic stiffness of a flexible connection on the elastic stiffness of a beam member are represented by the two stiffness matrices $\mathbf{S}(\mathbf{s}) \in \Re^{m\times m}$ and $\mathbf{S}_f(\mathbf{s}) \in \Re^{n\times n}$. These matrices are written as functions of stresses $\mathbf{s}$, so that the conventional linear stiffness relations no longer hold. Details of both matrices $\mathbf{S}$ and $\mathbf{S}_f$ are also stated in Appendix A.

Plastic strain rates $\dot{\mathbf{p}}$ are defined by an associative flow rule in (7), and expressed as functions of the plastic multiplier rates $\dot{\mathbf{z}} \in \Re^y$ through the constant matrix of outward normals $\mathbf{N} \in \Re^{m\times y}$ to the yield surface. Finally, the sign-constrained piecewise linear yield functions $\mathbf{w} \in \Re^y$ are defined through the hardening matrix $\mathbf{H} \in \Re^{y\times y}$ and appropriate yield limits $\mathbf{r} \in \Re^y$ in (8). Underpinning the description of the rate nonholonomic law in (8) is a "complementarity" mathematical structure. For vectors $\mathbf{w} \geqslant \mathbf{0}$ and $\dot{\mathbf{z}} \geqslant \mathbf{0}$, the complementarity condition is typically written as $\mathbf{w}^{\mathrm{T}}\dot{\mathbf{z}} = 0$. Mechanically, these constraints, as illustrated in Fig. 3a, allow for elastic unloading, and exclude the simultaneous activation and unloading of the same yield mode.

There are three ways in which the nonholonomic state problem can be formulated, all by simply collecting the basic set of relations (1)–(8). These three formats depend on which variables are retained to produce equivalent complementarity formulations, namely $(\mathbf{s}, \boldsymbol{\pi}_f, \mathbf{u}, \mathbf{z}, \dot{\mathbf{z}})$, $(\mathbf{u}, \mathbf{z}, \dot{\mathbf{z}})$ and $(\mathbf{z}, \dot{\mathbf{z}})$. At variance with other previous work (see, e.g. Franchi et al., 1981; Tin-Loi and Misa, 1996; Bolzon and Tin-Loi, 1999; Tangaramvong and Tin-Loi, 2010b) where the more compact form either in variables $(\mathbf{u}, \mathbf{z}, \dot{\mathbf{z}})$ or in variables $(\mathbf{z}, \dot{\mathbf{z}})$ is used, the present study adopts the most natural nonholonomic formulation in mixed static-kinematic variables $(\mathbf{s}, \boldsymbol{\pi}_f, \mathbf{u}, \mathbf{z}, \dot{\mathbf{z}})$. This is described as follows:

$$\begin{aligned}
&\mathbf{C}_0^{\mathrm{T}}\mathbf{s} + \mathbf{C}_f^{\mathrm{T}}\boldsymbol{\pi}_f - \alpha\mathbf{f} - \mathbf{f}_d = \mathbf{0},\\
&\mathbf{S}(\mathbf{s})\{\mathbf{C}_0\mathbf{u} - \mathbf{N}\mathbf{z}\} - \mathbf{s} = \mathbf{0},\\
&\mathbf{S}_f(\mathbf{s})\{\mathbf{C}_f\mathbf{u}\} - \boldsymbol{\pi}_f = \mathbf{0},\\
&\mathbf{w} = -\mathbf{N}^{\mathrm{T}}\mathbf{s} + \mathbf{H}\mathbf{z} + \mathbf{r} \geqslant \mathbf{0}, \quad \dot{\mathbf{z}} \geqslant \mathbf{0}, \quad \mathbf{w}^{\mathrm{T}}\dot{\mathbf{z}} = 0.
\end{aligned} \tag{9}$$

The complementarity system in (9) is a special instance of a mathematical program known as an MCP (Dirkse and Ferris, 1995a). The MCP, it is noted, is a generalization of the well-known linear complementarity problem (LCP) (Cottle et al., 1992), and is distinguished loosely from the LCP by the fact that it contains free variables. In view of the nonlinear stiffness matrices $\mathbf{S}$ and $\mathbf{S}_f$ describing the required 2nd-order geometry, this MCP (9) is nonlinear.

2.2.2. Holonomic state problem

The holonomic state problem can be essentially formulated in the same manner. However, all relations are now written in total quantities, as required by the path-independent assumption. In particular, relations (1)–(6) are retained, whilst (7) and (8) are replaced respectively by the following:

$$\mathbf{p} = \mathbf{N}\mathbf{z}, \tag{10}$$

$$\mathbf{w} = -\mathbf{N}^{\mathrm{T}}\mathbf{s} + \mathbf{H}\mathbf{z} + \mathbf{r} \geqslant \mathbf{0}, \quad \mathbf{z} \geqslant \mathbf{0}, \quad \mathbf{w}^{\mathrm{T}}\mathbf{z} = 0. \tag{11}$$

The holonomic associative flow rule is represented by (10) and path-independence is reflected by the complementarity relation (11) between the total quantities $\mathbf{w}$ and $\mathbf{z}$. This describes the fact that plastic yielding can only occur if the stress point is actually on the yield surface.

The governing holonomic state problem in variables $(\mathbf{s}, \boldsymbol{\pi}_f, \mathbf{u}, \mathbf{z})$ is given by the following nonlinear MCP:

$$\begin{aligned}
&\mathbf{C}_0^{\mathrm{T}}\mathbf{s} + \mathbf{C}_f^{\mathrm{T}}\boldsymbol{\pi}_f - \alpha\mathbf{f} - \mathbf{f}_d = \mathbf{0},\\
&\mathbf{S}(\mathbf{s})\{\mathbf{C}_0\mathbf{u} - \mathbf{N}\mathbf{z}\} - \mathbf{s} = \mathbf{0},\\
&\mathbf{S}_f(\mathbf{s})\{\mathbf{C}_f\mathbf{u}\} - \boldsymbol{\pi}_f = \mathbf{0},\\
&\mathbf{w} = -\mathbf{N}^{\mathrm{T}}\mathbf{s} + \mathbf{H}\mathbf{z} + \mathbf{r} \geqslant \mathbf{0}, \quad \mathbf{z} \geqslant \mathbf{0}, \quad \mathbf{w}^{\mathrm{T}}\mathbf{z} = 0.
\end{aligned} \tag{12}$$

3. Stepwise holonomic analysis

The mathematical programming based approach to trace robustly and effectively the complete (path-dependent) response of the elastoplastic structure in the simultaneous presence of connection semirigidity and 2nd-order geometry is briefly outlined in the following.

Our algorithm is based on the classical (small deformation) stepwise holonomic scheme (Maier, 1971; Franchi et al., 1981; Bird and Martin, 1990). In essence, the actual nonholonomic rate problem in (9) is replaced by its finite incremental counterpart. At variance with a nonholonomic approach, the incremental step is a priori fixed, and there is no need to identify exactly all critical events such as loading and unloading of stresses. Moreover, the adopted backward difference scheme does not limit the choice of the step size (Bird and Martin, 1990). Any violation of nonholonomy within each step is deemed to be acceptable. As found in our recent study (Tangaramvong and Tin-Loi, 2010b), a stepwise holonomic analysis is able to predict with sufficient accuracy the exact nonholonomic response, but with much less computational effort.

The entire evolution of the nonholonomic structural response is thus approximated as a sequence of finite incremental holonomic problems. Each problem concerns a configuration change $\Delta\Sigma$ from a previously known state $\bar{\Sigma}$, which involves known variables (e.g. $\bar{\alpha}, \bar{\mathbf{s}}, \bar{\boldsymbol{\pi}}_f, \bar{\mathbf{u}}, \bar{\mathbf{z}}$), to the current unknown state $\Sigma = \bar{\Sigma} + \Delta\Sigma$. For a predefined finite incremental step $\Delta\alpha$, the incremental response variables $(\Delta\mathbf{s}, \Delta\boldsymbol{\pi}_f, \Delta\mathbf{u}, \Delta\mathbf{z})$ that will develop during the configuration change $\Delta\Sigma$ are calculated. It is clear that

$$\alpha = \bar{\alpha} + \Delta\alpha, \quad \mathbf{s} = \bar{\mathbf{s}} + \Delta\mathbf{s}, \ldots \tag{13}$$

Therefore, the finite step problem in variables $(\Delta\mathbf{s}, \Delta\boldsymbol{\pi}_f, \Delta\mathbf{u}, \Delta\mathbf{z})$ can be formulated by simply substituting (13) and $\dot{\mathbf{z}} = \Delta\mathbf{z}$ into the appropriate nonholonomic relation (9) to give the following:

$$\begin{aligned}
&\mathbf{C}_0^{\mathrm{T}}(\bar{\mathbf{s}} + \Delta\mathbf{s}) + \mathbf{C}_f^{\mathrm{T}}(\bar{\boldsymbol{\pi}}_f + \Delta\boldsymbol{\pi}_f) - (\bar{\alpha} + \Delta\alpha)\mathbf{f} - \mathbf{f}_d = \mathbf{0},\\
&\mathbf{S}(\bar{\mathbf{s}} + \Delta\mathbf{s})\{\mathbf{C}_0(\bar{\mathbf{u}} + \Delta\mathbf{u}) - \mathbf{N}(\bar{\mathbf{z}} + \Delta\mathbf{z})\} - (\bar{\mathbf{s}} + \Delta\mathbf{s}) = \mathbf{0},\\
&\mathbf{S}_f(\bar{\mathbf{s}} + \Delta\mathbf{s})\{\mathbf{C}_f(\bar{\mathbf{u}} + \Delta\mathbf{u})\} - (\bar{\boldsymbol{\pi}}_f + \Delta\boldsymbol{\pi}_f) = \mathbf{0},\\
&\mathbf{w} = -\mathbf{N}^{\mathrm{T}}(\bar{\mathbf{s}} + \Delta\mathbf{s}) + \mathbf{H}(\bar{\mathbf{z}} + \Delta\mathbf{z}) + \mathbf{r},\\
&\mathbf{w} \geqslant \mathbf{0}, \quad \Delta\mathbf{z} \geqslant \mathbf{0}, \quad \mathbf{w}^{\mathrm{T}}\Delta\mathbf{z} = 0,
\end{aligned} \tag{14}$$

where the two matrices $\mathbf{S}$ and $\mathbf{S}_f$ are written as functions of unknown stresses $\Delta\mathbf{s}$ (see Appendix A).

The actual nonholonomic problem (9) is thus replaced by a series of finite step holonomic problems, each represented by the nonlinear MCP (14). Since a regular progression of yielding is assumed for any step (such that any elastic unloading is ruled out within that step) unloading is captured at the beginning of a new step. With such a step-by-step approach the structural response can be traced accurately provided that the steps are sufficiently small and that unloading does not occur extensively, as is invariably the case for actual structures.

The novelty of our proposed algorithm, as alluded to earlier, lies in the fact that, even in the presence of geometric nonlinearity, an iterative approach such as the ubiquitous predictor–corrector scheme (e.g. Kassimali, 1983; Forde and Stiemer, 1987; Comi and Maier, 1990; Tin-Loi and Misa, 1996; Tangaramvong and Tin-Loi,

2010b) is not required. Instead, we process, for each configuration change $\Delta\bar{\Sigma}$, the MCP (14) directly using the state-of-the-art complementarity solver GAMS/PATH (Dirkse and Ferris, 1995b) from within the mathematical programming environment GAMS (Brooke et al., 1998). GAMS is an acronym for General Algebraic Modeling System.

Our complete algorithmic approach is described in the following.

Step (0): Initialization
- Set stopping criteria: load level, maximum number of equilibrium paths, etc.
- Define the finite step length Δt (positive scalar).
- At $\bar{\Sigma} = 0$, initialize variables (e.g. $\alpha = 0$, $\mathbf{s} = \mathbf{0}$, $\boldsymbol{\pi}_f = \mathbf{0}$, $\mathbf{z} = \mathbf{0}$ and $\mathbf{w} = \mathbf{r}$). Go to Step (a).

Step (a): Solve finite step problem
- Solve MCP (14) either for the prescribed $\mathbf{f}_d$ (with $\Delta\alpha = 0$) or for two finite increments (namely $\Delta\alpha = \Delta t$ and $\Delta\alpha = -\Delta t$).
- Collect all multiple solutions (if they exist) and select one solution.
- Form the new stress state $\bar{\Sigma}$, and update according to (13). Go to Step (b).

Step (b): Check termination
- If the termination criterion has been reached, or all solutions found at Step (a) have been exhausted, stop.
- Else, return to Step (a) either to proceed with the current state $\bar{\Sigma}$ or to choose an unexplored solution found previously.

Some additional remarks regarding the proposed stepwise holonomic algorithm are:

(a) Rather than processing the MCP (14) using all yield modes, our implementation adopts a prediction of yield hyperplanes that are likely to be active during the particular incremental step (Ardito et al., 2008; Tangaramvong and Tin-Loi, 2010b). This special technique allows a partition of the MCP into potential active and nonactive yield sets, and thus leads to significant reductions in complementarity size and hence of computational cost.

(b) In view of geometric nonlinearity, bifurcation leading to multiple equilibrium paths can be expected at any load level. The strategy proposed to detect this event is to simply test for both $\Delta\alpha = \Delta t$ and $\Delta\alpha = -\Delta t$ at the MCP solve. Multiple solutions (if they exist) are captured by using a special enumerative scheme (Tin-Loi et al., 2007) at Step (a).

(c) A limit point is recognized when application of $\Delta\alpha = \Delta t$ does not yield any solution. To identify closely this point, our implementation applies an automatic refinement of the finite step Δt reduced by a factor of 0.5 (until $\Delta t \leqslant 10^{-5}$) when the maximum load capacity is approached.

4. Extended limit analysis

The aim of our extended analysis is similar to that of the classical approach, namely to obtain in a single step a bound to the maximum load. However, in our case ductility constraints and 2nd-order geometric effects are included. Various other quantities of interest corresponding to that load, such as displacements $\mathbf{u}$ and stresses $\mathbf{s}$, can be obtained as by-products.

Our extended limit analysis approach is based on holonomic conditions. This assumption, as reported by Tangaramvong and Tin-Loi (2007), is reasonable for realistic structures since their global responses computed on the basis of holonomy closely predict those from the actual nonholonomic assumption.

The idea underpinning our analysis is simple: since the holonomic formulation given by the nonlinear MCP (12) provides the complete basic ingredients that govern the structural behavior for the entire proportionally applied load history, the very same relations can be used to formulate the extended limit analysis problem. At variance with a holonomic elastoplastic analysis for which the load multiplier α is known a priori, the limit analysis assumes that α is variable. The aim is then to maximize α subject to the holonomic constraints.

In view of the foregoing remarks, the extended limit analysis can be expressed as the following optimization problem in variables $(\alpha, \mathbf{s}, \boldsymbol{\pi}_f, \mathbf{u}, \mathbf{z})$:

$$\begin{aligned} &\text{maximize} && \alpha \\ &\text{subject to} && \text{MCP (12)}, \\ & && \text{ductility constraints}, \end{aligned} \tag{15}$$

where "ductility constraints" impose generally limits on such quantities as total displacements at some specific points of structures, rotation capacities, etc. Problem (15) is an instance of the optimization class known as an MPEC (Luo et al., 1996), for which equilibrium constraints are in fact complementarity constraints. This type of optimization problem has increasingly attracted research interest due to the fact that, in addition to being theoretically difficult and computationally challenging, MPECs find numerous applications in both economic and engineering problems involving equilibrium systems (Ferris and Pang, 1997).

The systematic study of MPECs is a relatively new field of mathematical programming. The most prominent feature of an MPEC, and one that distinguishes it from a standard NLP problem, is the presence of complementarity constraints. These constraints classify the MPEC as a nonlinear disjunctive program. Besides the common issues associated with general NLP problems, the MPEC is complicated by a "combinatorial curse". Whilst an extensive theory of first and second order optimality conditions for an MPEC has been developed (Luo et al., 1996), still relatively little is known about the numerical solution of practical, large-scale MPECs likely to arise in realistic applications. To date, there are unfortunately no known numerical algorithms guaranteed to solve such an MPEC.

There are three main reasons for the difficulty of solving MPECs such as the one given by (15): they are disjunctive in view of the embodied complementarity conditions (namely, either $w_j = 0$ or $z_j = 0$); the feasible region of the MPEC may not be convex; and the feasible solution space may not be connected. Any of these can lead to severe numerical instability.

An attempt to directly solve the MPEC, such as the one defined by (15), would typically suffer from numerical difficulties, and is likely to succeed only small size problems (Cocchetti and Maier, 2003). A far better approach is to transform the MPEC into a standard NLP problem, for which the nonconvex and nonsmooth complementarity constraints are parameterized. This reformulated MPEC is then solved as a series of NLP subproblems such that the original complementarity condition is approached, as the governing positive parameter (μ) is increased or decreased. The attraction of this scheme is that each subproblem is a standard NLP problem, and general purpose industry standard NLP codes, such as GAMS/CONOPT (Drud, 1994), can be employed.

In the following, we briefly outline three basic algorithms we have used with varying degrees of success. They are categorized by the way complementarity is treated.

1. *Penalization*: The complementarity term is transferred to the objective function and penalized (see, e.g. Ferris and Tin-Loi, 1999). More explicitly, this involves adding the term $-\mu\mathbf{w}^{\mathrm{T}}\mathbf{z}$ to the objective function. A negative penalization, it is noted,

is required in view of the maximization process. At each NLP iterate, the algorithm increases the penalty parameter μ until complementarity is satisfied to within some preset tolerance.

2. *Smoothing*: The algorithm replaces the term $\mathbf{w}^T\mathbf{z} = 0$ by appropriate smoothing functions $\psi_\mu(w_j, z_j) = 0$ for all j. The particular one often used is the well-known Fischer–Burmeister function (Kanzow, 1996):

$$\psi_\mu(w_j, z_j) = \sqrt{w_j^2 + z_j^2 + 2\mu} - (w_j + z_j). \tag{16}$$

The function ψ_μ has the property that $\psi_\mu(w_j, z_j) = 0$ if and only if $w_j \geqslant 0$, $z_j \geqslant 0$ and $w_j z_j = \mu$. The parameterization ψ_μ is a smoothing of the mapping $\psi_{\mu=0}$ implying that it is differentiable for nonzero μ. The algorithm processes a series of NLP subproblems that iteratively decrease the smoothing parameter μ in order to drive the complementarity term to zero (see, e.g. Tin-Loi and Que, 2001).

3. *Relaxation*: The complementarity constraint $\mathbf{w}^T\mathbf{z} = 0$ is replaced by its relaxed version $\mathbf{w}^T\mathbf{z} \leqslant \mu$. This relaxed problem is successively solved for smaller values of μ to enforce the complementarity term to zero (see, e.g. Ferris and Tin-Loi, 2001).

We can make three comments on these approaches for solving our extended limit analysis problem:

(a) For all the problems we tested, the three proposed parameterizations had no difficulties whatsoever in processing successfully MPEC (15). The penalty algorithm appears to be the most robust and efficient MPEC solution scheme, and hence has been adopted in the present study. The particular algorithmic implementation involves iteratively solving the following NLP subproblem in variables $(\alpha, \mathbf{s}, \boldsymbol{\pi}_f, \mathbf{u}, \mathbf{z})$:

$$\begin{aligned} \text{maximize} \quad & \alpha - \mu\mathbf{w}^T\mathbf{z} \\ \text{subject to} \quad & \mathbf{C}_0^T\mathbf{s} + \mathbf{C}_f^T\boldsymbol{\pi}_f - \alpha\mathbf{f} - \mathbf{f}_d = \mathbf{0}, \\ & \mathbf{S}(\mathbf{s})\{\mathbf{C}_0\mathbf{u} - \mathbf{N}\mathbf{z}\} - \mathbf{s} = \mathbf{0}, \\ & \mathbf{S}_f(\mathbf{s})\{\mathbf{C}_f\mathbf{u}\} - \boldsymbol{\pi}_f = \mathbf{0}, \\ & \mathbf{w} = -\mathbf{N}^T\mathbf{s} + \mathbf{H}\mathbf{z} + \mathbf{r} \geqslant \mathbf{0}, \quad \mathbf{z} \geqslant \mathbf{0}, \\ & \text{ductility constraints}, \end{aligned} \tag{17}$$

for successively higher values of μ until a preset tolerance on the complementarity condition (i.e. $\mathbf{w}^T\mathbf{z} \leqslant 10^{-6}$) is met. The adopted starting values of μ are in all cases $\mu = 1$, and are updated after each NLP solve by $\mu = 10\mu$.

(b) In the presence of geometric nonlinearity, the constraints (17) are nonlinear since the two matrices $\mathbf{S}$ and $\mathbf{S}_f$ are expressed as functions of stresses $\mathbf{s}$ (see Appendix A). Once again, rather than adopting some cumbersome iterative procedure to achieve convergence, our proposed algorithm processes each subproblem (17) directly using the NLP solver GAMS/CONOPT. This advantageously provides a significant reduction in computational effort by eliminating the typical outer level iterative routines.

(c) The optimization problem given by the MPEC (15) can strictly only guarantee an upper bound solution to the maximum load. Successful numerical solution will in fact provide the largest upper bound. An upper bound solution is achieved when there are multiple limit loads, associated with multiple equilibrium paths. In practice, however, the exact limit load is often captured as when a single equilibrium branch exists, as for realistic structures (see, e.g. Tangaramvong and Tin-Loi, 2007, 2010b). For such cases, the exact load is hence computed.

5. Illustrative examples

Four numerical examples are provided to illustrate application of the proposed stepwise holonomic and extended limit analysis approaches. All examples involve realistic elastoplastic frames with semirigid beam-to-column connections (denoted as opened square dots) considering also the effects of 2nd-order geometry.

The first example is a typical unbraced frame model for a Winnipeg office building (Frye and Morris, 1975; Misa, 1995). This example provides some validation of the accuracy of the stepwise holonomic approach and demonstrates the fact that numerical stability is achieved with our proposed algorithm, even for large step sizes. The second and third examples are benchmark problems provided by Anderson and Kavianpour (1991) and Galea et al. (1988), respectively. The last example is a reasonably sized multistory braced frame (Tangaramvong and Tin-Loi, 2009b, 2010a).

Piecewise linearized yield surfaces were adopted in all cases. For an I-steel section under combined bending and axial force, "start" hinge a of an element i is then the hexagonal piecewise linear yield diagram shown in Fig. 5a, where $\tan\gamma = 1/0.85$, $r_b = 0.15$ and s_{1u} defines the axial yield capacity. Positive and negative flexural/axial properties are assumed to be identical. A multilinear diagram (Fig. 5b) was used to suitably represent the general nonlinear moment–rotation behavior of semirigid connections, where M_j and K_j^a define the corresponding flexural capacity and slope for each linear portion j, respectively. Mathematical descriptions underpinning the inelastic constitutive laws are provided in (7), (8) and (10), (11) for nonholonomic and holonomic behaviors, respectively. Explicit expressions of key vectors and matrices are given in Appendix B.

Both the proposed stepwise holonomic and extended limit analysis algorithms have been implemented as MATLAB codes, linked to the GAMS mathematical programming environment by a MATLAB-GAMS interface (Ferris, 1998). The step-by-step behavior was traced using the stepwise holonomic algorithm with GAMS/PATH (Dirkse and Ferris, 1995b) as the MCP solver. For the MPEC runs, the penalty NLP based algorithm was implemented, and the NLP solves were carried out using the robust GAMS/CONOPT optimization code (Drud, 1994). The reported CPU times are for a 3 GHz Pentium PC with 4 GB RAM, running WinXP.

5.1. Example 1: 11 story portal frame

The first example concerns the 11 story steel portal frame in Fig. 6. It is subjected to vertical and lateral forces (kips) defined in terms of a load multiplier α as shown in Fig. 6, where v denotes the corresponding top story sway displacement (in). This frame was initially modeled for a Winnipeg office building by Frye and

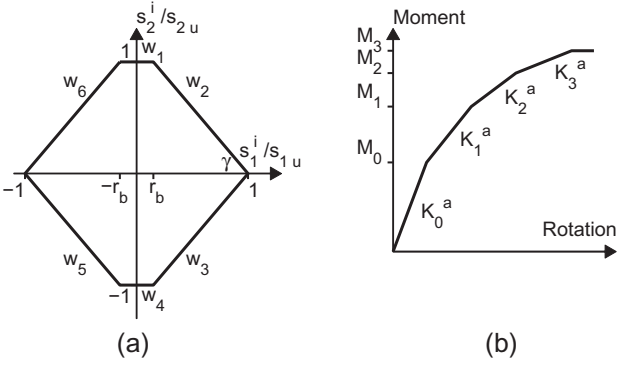

Fig. 5. Piecewise linear models: (a) interaction between flexural and axial forces and (b) moment-rotation relation for flexible connections.

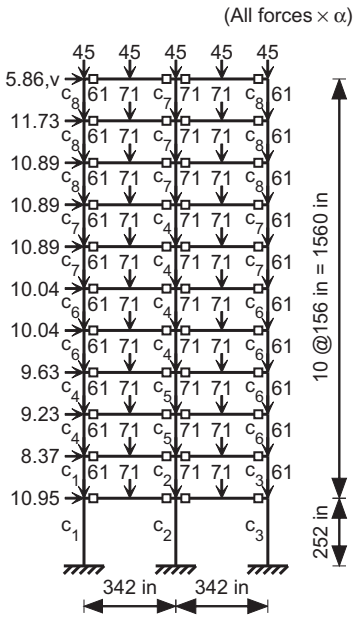

Fig. 6. Example 1: 11 story portal frame.

Morris (1975) to examine the influence of nonlinear flexible connections. However, both material and geometric linearities were assumed. Later, Misa (1995) analyzed the same frame using a nonholonomic elastoplastic analysis (using an iterative predictor–corrector scheme) and allowing for arbitrarily large deformations.

We carried out the following five analyses:

- Case a: Stepwise holonomic analysis, rigid connections, geometric linearity.
- Case b: Stepwise holonomic analysis, semirigid connections, geometric linearity.
- Case c: Stepwise holonomic analysis, rigid connections, 2nd-order geometry.
- Case d: Stepwise holonomic analysis, semirigid connections, 2nd-order geometry.
- Case e: Extended limit analysis, semirigid connections, 2nd-order geometry, limited displacement of $-7.248 \leqslant v \leqslant 7.248$ (in).

Material properties adopted were WF sections with $E = 29{,}000$ ksi: W21 × 83 for all beams, $s_{2u} = 7056$ kip-in. For columns, eight different sections indicated as c_1 to c_8 in Fig. 6 were employed: namely W14 × 342 for c_1, $s_{2u} = 24231.31$ kip-in, $s_{1u} = 3638.16$ kips; W14 × 398 for c_2, $s_{2u} = 28866.67$ kip-in, $s_{1u} = 4212.9$ kips; W14 × 287 for c_3, $s_{2u} = 19508.07$ kip-in, $s_{1u} = 2996.46$ kips; W14 × 264 for c_4, $s_{2u} = 17497.95$ kip-in, $s_{1u} = 2723.04$ kips; W14 × 314 for c_5, $s_{2u} = 21700.53$ kip-in, $s_{1u} = 3292.2$ kips; W14 × 219 for c_6, $s_{2u} = 14002.75$ kip-in, $s_{1u} = 2232$ kips; W14 × 176 for c_7, $s_{2u} = 11555.46$ kip-in, $s_{1u} = 1863.72$ kips; and W14 × 120 for c_8, $s_{2u} = 7649.45$ kip-in, $s_{1u} = 1272.24$ kips.

As is typical, yielding in all beams was assumed to form under pure bending, whilst the combined stress model in Fig. 5a was adopted for all columns. For semirigid bolted T-stub beam-to-column connections, we assumed the multibranch moment–rotation (kip-in, rad × 10^{-3}) diagram shown in Fig. 5b with a linearization of: (0,0), (1620,0.58), (3480,3.30), (5520,9.30) and (7056,16.90). The discretized frame model consisted of 77 members, 58 nodes, 165 degrees of freedom, and 572 (for rigid connection Cases a and c) or 704 (for semirigid connection Cases b, d and e) yield functions.

The accuracy of our 2nd-order geometry, stepwise holonomic approach (Case d) to predict the overall response of the semirigid frame can be assessed by comparison with the results of Misa (1995) who performed an exact nonholonomic analysis allowing for arbitrarily large deformations. Our stepwise holonomic analyses, carried out for different step sizes (namely $\Delta t = 0.02$, 0.1, 0.2 and 0.4, using respectively CPU times of 248, 229, 301 and 301 s) matched very well, as shown in Fig. 7, the exact response. We should also note that, for this structure, only a single equilibrium path exists, and we accurately estimated the maximum load by our implemented automatic load step refinement. Computationally, our algorithm performed very well as it did not have any convergence difficulties even for the largest step size adopted. Unstable equilibrium paths were also robustly traced. As expected, the numerous hinge unloadings identified did not significantly affect the overall response of the structure. A stepwise holonomic approach, as previously indicated, does not capture exactly all critical events; these all are identified in the same or subsequent steps. For instance, for the stepwise holonomic Case d response (Fig. 7, $\Delta t = 0.02$), we identified the first partial hinge at some flexible beam joint when $\alpha \approx 0.26$. Yielding due to combined stresses first occurred at some base column when $\alpha \approx 1.22$. At the same load ($\alpha \approx 1.22$), some beam joint attained full plasticity. The first unloading was detected at some flexible connection when $\alpha \approx 1.245$. The maximum load capacity was reached at approximately $\alpha_{max} \approx 1.249$.

The structure responses for each of the stepwise holonomic Cases a–d ($\Delta t = 0.02$) are shown in Fig. 8. The CPU times spent to analyze these Cases a–c were 41, 67 and 252 s, respectively. Hinge dispositions corresponding to the maximum load for each case are depicted in Fig. 9. It can be observed that from an early phase, significant amount of lateral displacement is produced due to the effect of semirigid connections. Under the geometrically linear assumption, the maximum loads of $\alpha_{max} \approx 1.644$ (for rigid frame Case a) and of $\alpha_{max} \approx 1.642$ (for semirigid frame Case b) are approached at approximately the same level. Both analyses were terminated due to an excessive sway displacement of $v = 70$ in. However, in the presence of geometric nonlinearity, the influence of flexible connections became more dominant since they further reduced (some 6%) the load carrying capacity of the structure, as can be seen by comparing the maximum load of the semirigid frame Case d ($\alpha_{max} \approx 1.249$) with the rigid frame Case c ($\alpha_{max} \approx 1.327$). At the limit point for Case d, the hinge dispositions (Fig. 9d) indicate that only few flexible joints have attained full plasticity. As expected, beyond their limit points, both frames in Cases c and d lost significantly their load carrying capacities as their response entered the softening (unstable) equilibrium path.

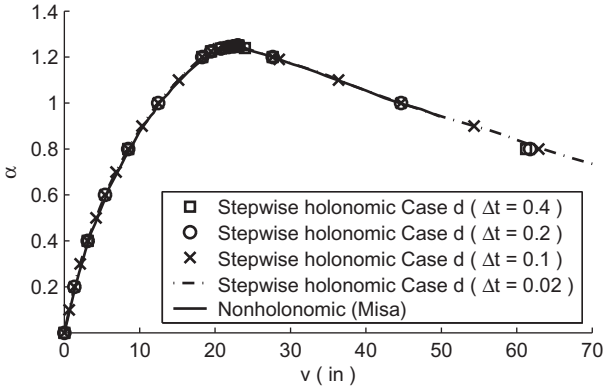

Fig. 7. Example 1: $\alpha - v$ responses for stepwise holonomic and nonholonomic (Misa, 1995) analyses.

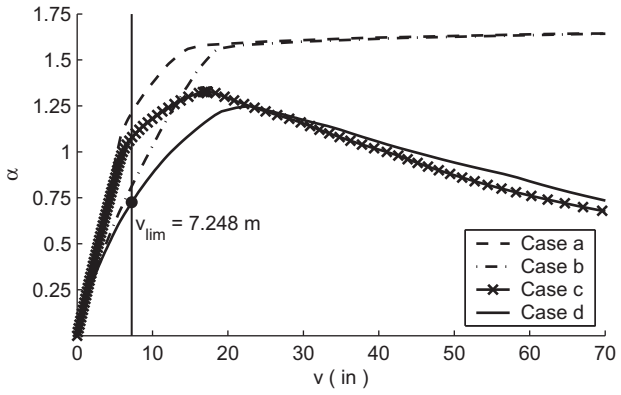

Fig. 8. Example 1: stepwise holonomic $\alpha - v$ responses.

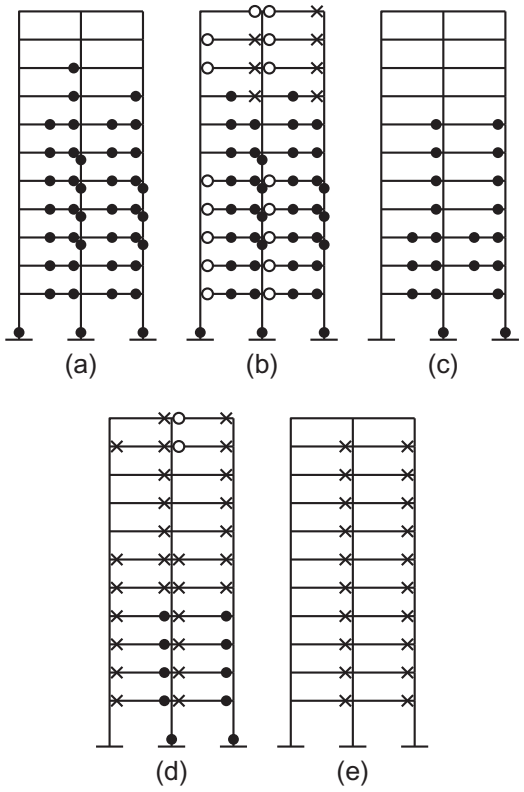

Fig. 9. Example 1: hinge dispositions at limit load (a) Case a, (b) Case b, (c) Case c, (d) Case d and (e) Case e (• denotes fully plastic hinge, × partially plastic hinge and ○ unloaded hinge).

The extended ductility constrained limit analysis (Case e) was successfully solved in a single step using the proposed MPEC approach. The CPU time used was about 1 s. The maximum load computed, namely $\alpha_{max} = 0.725$ with $v = 7.248$ in, is plotted as a dot on the corresponding Case d stepwise holonomic behavior in Fig. 8. This limit analysis result is clearly in accord with our evolutive analysis, and it also satisfies the imposed displacement constraint (thin line). Hinge dispositions at the computed peak load are displayed in Fig. 9e.

5.2. Example 2: 3 story portal frame

The 3 story, single bay semirigid structure in Fig. 10 is a benchmark example (Anderson and Kavianpour, 1991) often used to validate the accuracy of developed analysis methods for semirigid

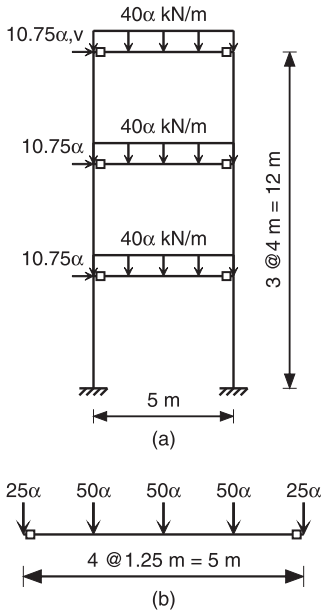

Fig. 10. Example 2: 3 story portal frame: (a) structure and loading and (b) beam discretization.

frames. This structure is subjected to uniformly distributed loads of 40α kN/m on the beams and lateral loads of 10.75α kN, where v denotes the corresponding top sway displacement (m).

The frame is made up of steel sections (HEB200 for all columns, $s_{2u} = 151$ kN m, $s_{1u} = 1835.35$ kN, and IPE300 for all beams, $s_{2u} = 147.6$ kN m) with $E = 2 \times 10^8$ kN m^{-2}. All beam-to-column connections are semirigid with the idealized multilinear moment–rotation (kN m, rad $\times 10^{-3}$) shown in Fig. 5b, with breakpoints at (0,0), (75,4), (97.5,11.8), (107.5,24.4) and (120,60.4). As usual, we assumed that beams could yield under pure bending and columns under combined stresses (Fig. 5a). Our beam discretization is shown in Fig. 10b, leading to a model consisting of 18 members, 17 nodes, 45 degrees of freedom and 138 yield functions.

The full history of $\alpha - v$ responses, including the effects of 2nd-order geometry, was successfully traced using our stepwise holonomic scheme, with $\Delta t = 0.2$. The total CPU time consumed was about 36 s. As expected for this realistic frame, there exists only a single equilibrium path (see Fig. 11). Obviously, the present results are in good agreement with the numerical results reported by Anderson and Kavianpour (1991), thus validating the accuracy of our proposed algorithm. The maximum load capacity was reached at approximately $\alpha_{max} \approx 1.635$, with the corresponding hinge dispositions shown in Fig. 12.

Our extended limit analysis took less than 1 s CPU time. The computed maximum load capacity was $\alpha_{max} = 1.635$ with $v = 0.256$ m. This value is plotted (as an open dot) on the associated stepwise holonomic response in Fig. 11. The obtained result clearly predicts accurately the load carrying capacity of the structure. It also incidentally provides the same hinge dispositions (Fig. 12) as those of the stepwise holonomic analysis.

5.3. Example 3: multi bay portal frame

The third example is that of a 2 story, 3 bay calibration frame (Fig. 13), originally analyzed by Galea et al. (1988). The frame is subjected to a uniformly distributed load of 40α kN/m on beams as well as lateral loads of 5α kN applied as shown; v indicates a top story sway displacement. Each column has an initial vertically imperfection of 1/300.

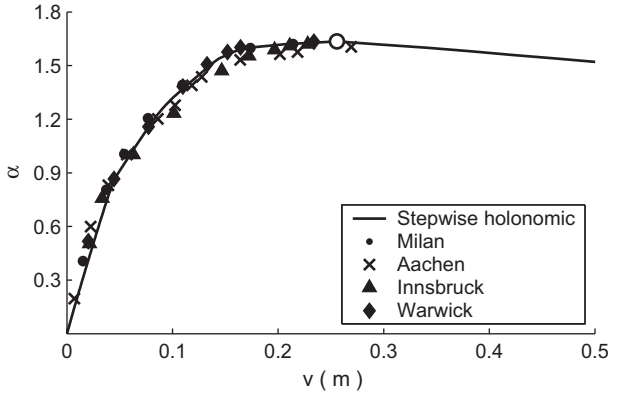

Fig. 11. Example 2: comparison of $\alpha - v$ response for stepwise holonomic analysis and other numerical results in Anderson and Kavianpour (1991).

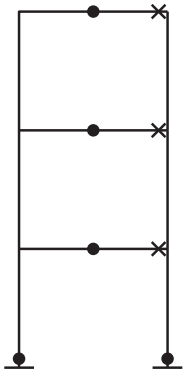

Fig. 12. Example 2: hinge dispositions at peak load (• denotes fully plastic hinge and × partially plastic hinge).

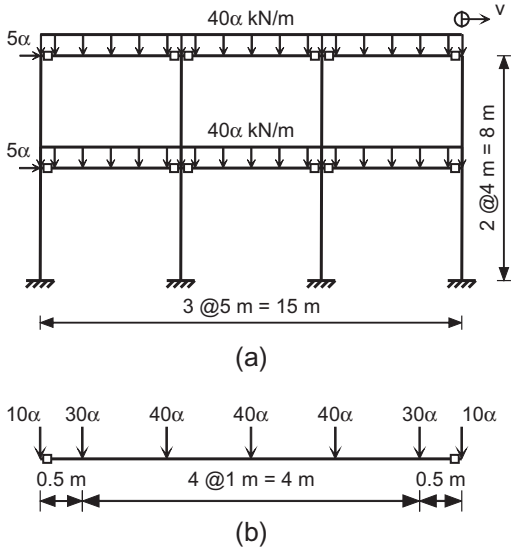

Fig. 13. Example 3: multi bay portal frame: (a) structure and loading and (b) beam discretization.

Four analysis cases were carried out as follows:

Case a: Stepwise holonomic analysis, rigid connections, geometric linearity.
Case b: Stepwise holonomic analysis, rigid connections, 2nd-order geometry.
Case c: Stepwise holonomic analysis, semirigid connections, 2nd-order geometry.
Case d: Extended limit analysis, semirigid connections, 2nd-order geometry, limited displacement of $-0.032 \leqslant v \leqslant 0.032$ (m).

The following steel sections ($E = 2 \times 10^8$ kN m^{-2}) were adopted: IPE300 for all beams, $s_{2u} = 147.6$ kN m; and HEA160 for all columns, $s_{2u} = 57.58$ kN m, $s_{1u} = 911.8$ kN. Yielding under pure bending was assumed for all beams and under combined stresses for all columns (Fig. 5a). The flexible connection analysis Cases c and d employed the multibranch moment–rotation (kN m, rad $\times 10^{-3}$) law shown in Fig. 5b: (0,0), (31,3.34), (42.50,6.30), (47.50,13.05) and (49.50,42.44). This is a linearized approximation of the actual nonlinear curve of Galea et al. (1988). The discretized finite element model, involving the beam discretization shown in Fig. 13b, consisted of 44 members, 42 nodes, 114 degrees of freedom, and 240 (for rigid joint Cases a and b) or 276 (for semirigid joint Cases c and d) yield functions.

For all stepwise holonomic Cases a–c, the complete $\alpha - v$ responses shown in Fig. 14 were traced using the proposed algorithm with $\Delta t = 0.02$. The CPU times were 22, 76 and 127 s for Cases a–c, respectively. For each of the analysis Cases a–c, there was only a single equilibrium path. Clearly, the present results for Case c provide a good correlation with the benchmark results (Galea et al., 1988). The small differences observed are most likely due to the assumed approximate piecewise linear moment–rotation diagram.

The influence of geometric nonlinearity is evident by comparing, for example, the responses of the 2nd-order geometry Case b and of the geometrically linear Case a. As expected, inclusion of geometric effects reduces the overall load carrying capacity of the structure. The 2nd-order geometry Case b graph starts to deviate from the small deformation Case a when the structure is still elastic. The maximum load capacity obtained for Case b ($\alpha_{max} \approx 1.745$) is approximately 14% less that of Case a ($\alpha_{max} \approx 1.989$). The corresponding hinge dispositions shown in Fig. 15 reveal that some plastic hinges that initially formed at some beams and columns in Case a do not actually occur in Case b. In the present instance, 2nd-order effects also produced a softening post peak behavior.

For the flexible connection Case c, the $\alpha - v$ response in Fig. 14 shows a further (significant) reduction in the maximum load

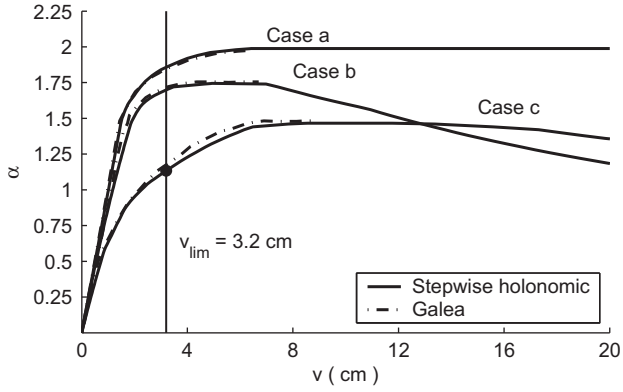

Fig. 14. Example 3: comparison of $\alpha - v$ responses for stepwise holonomic analyses and benchmark results (Galea et al., 1988).

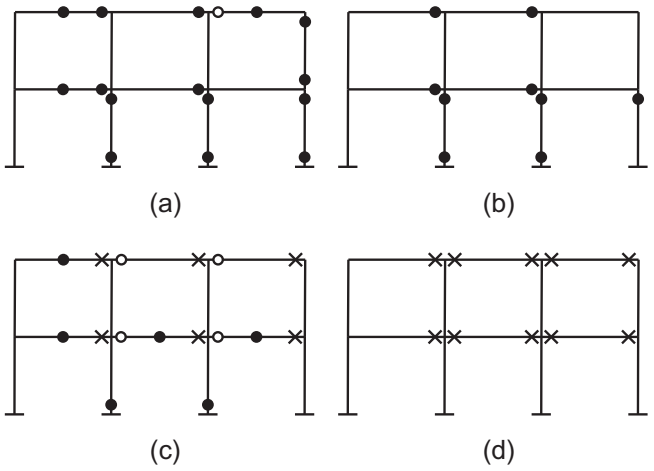

Fig. 15. Example 3: hinge dispositions at limit load: (a) Case a, (b) Case b, (c) Case c and (d) Case d (• denotes fully plastic hinge, × partially plastic hinge and ◦ unloaded hinge).

capacity, as compared to the rigid connection Case b. Not only was the peak load ($\alpha_{max} \approx 1.466$) attained at about 19% lower level than Case b, its associated sway displacement ($v \approx 0.118$ m) also increased dramatically. The corresponding hinge dispositions shown in Fig. 15c indicate that none of semirigid connections had yet developed full plasticity. Instead, elastic unloadings were detected at some of these joints.

The extended limit analysis Case d provided a maximum load of $\alpha_{max} = 1.133$ with a corresponding $v = 0.032$ m, in less than 1 s CPU time. This result is plotted as a dot on the associated stepwise holonomic Case c response (Fig. 14). Clearly, the required serviceability condition (thin line) is satisfied. Hinge dispositions corresponding to this load are depicted in Fig. 15d.

5.4. Example 4: 14 story braced frame

The last example concerns the 14 story, 3 bay braced frame shown in Fig. 16. This practical frame was originally used to investigate the influence of softening plasticity and 2nd-order geometry on its holonomic structural behavior (Tangaramvong and Tin-Loi, 2009b, 2010a). The frame was subjected to vertical loads of 5α (kN) and increasing lateral forces (kN) governed by the load factor α as shown, where v denotes the corresponding top sway displacement (m).

Three analysis cases were carried out as follows:

- Case a: Stepwise holonomic analysis, rigid connections, 2nd-order geometry.
- Case b: Stepwise holonomic analysis, semirigid connections, 2nd-order geometry.
- Case c: Extended limit analysis, semirigid connections, 2nd-order geometry, limited displacement of $-0.224 \leqslant v \leqslant 0.224$ (m).

Steel sections with $E = 2 \times 10^8$ kN m^{-2} were adopted: 350WC258 for all columns, $s_{2u} = 1246$ kN m, $s_{1u} = 9212$ kN; 200UC59.5 for all braces, $s_{2u} = 197$ kN m, $s_{1u} = 2286$ kN; and 410UB59.7 for all beams, $s_{2u} = 360$ kN m. Plasticity in all beams was assumed to form under pure bending, whilst yielding of all columns and braces accommodated the effects of combined axial and flexural forces (Fig. 5a). For the analysis Cases b and c, bay 1 and 3 beam-to-column connections were assumed to be semirigid; each followed the multibranch moment–rotation (kN m, rad $\times 10^{-3}$) diagram shown in Fig. 5b, with breakpoints at (0,0), (112,3.33), (163,8.54), (193,15.9) and (216,25.5). The discretized model consisted of 196 members, 130 nodes, 378 degrees of freedom, and 1456 (for the rigid connection Case a) or 1624 (for the flexible connection Cases b and c) yield functions.

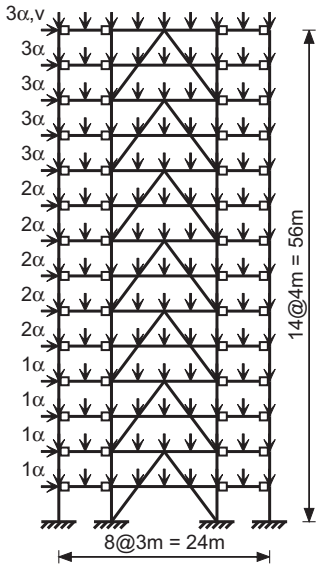

Fig. 16. Example 4: 14 story braced frame.

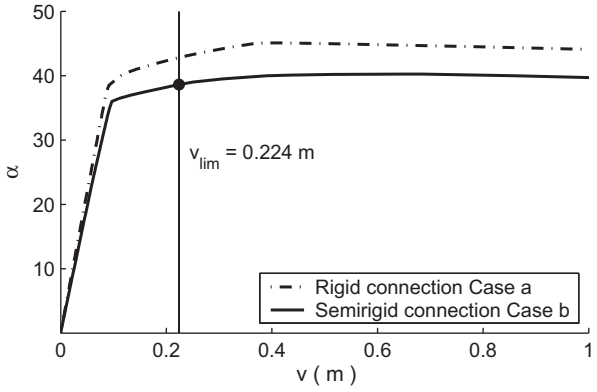

Fig. 17. Example 4: stepwise holonomic $\alpha - v$ responses.

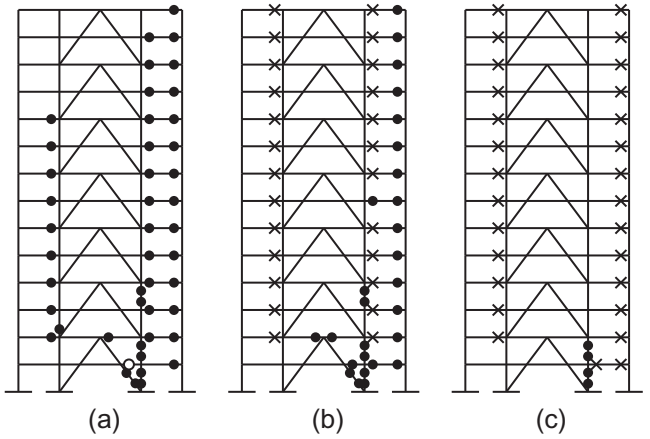

Fig. 18. Example 4: hinge dispositions at limit load: (a) Case a, (b) Case b and (c) Case c (• denotes fully plastic hinge, × partially plastic hinge and ◦ unloaded hinge).

In Cases a and b, the stepwise holonomic $\alpha - v$ responses, computed with $\Delta t = 0.5$, are shown in Fig. 17. The corresponding CPU times were 763 and 1336 s for Cases a and b, respectively. Hinge dispositions corresponding to the maximum load for each of the Cases a and b are plotted in Fig. 18. The results were as expected: in the presence of geometric nonlinearity, the effect of semirigidity not only decreased the peak load, but also increased the deflections. As compared to the rigid connection Case a ($\alpha_{max} \approx 45.099$ at $v \approx 0.415$ m), some 12% reduction in the maximum load and a larger sway displacement were obtained for the semirigid connection Case b ($\alpha_{max} \approx 40.256$ at $v \approx 0.686$ m).

Our extended limit analysis under displacement constraints successfully predicted, in 6 s CPU time, a maximum load of $\alpha_{max} = 38.608$ with $v = 0.224$ m. This result is plotted as a dot on the associated stepwise holonomic Case b response. It clearly satisfies the imposed deflection (thin line) limit. Corresponding hinge dispositions to the limit load are shown in Fig. 18c.

6. Concluding remarks

This paper presents robust and efficient mathematical programming based approaches to carry out evolutive and extended limit analyses for the safety assessment of elastoplastic frames for which some or all of the beam-to-column connections are semirigid. The influence of material and geometric nonlinearities are simultaneously accommodated. For computational efficiency and without undue loss of accuracy, the evolutive analysis is carried out in a stepwise holonomic fashion. Our extended limit analysis, similar to a classical analysis, aims at obtaining in a single step a bound to the maximum load capacity. Moreover, it can also account for nonperfect plasticity, geometric nonlinearities and limited ductility conditions.

The novelty of our stepwise holonomic algorithm is that it is processed without the use of any iterative, typically some predictor–corrector type, algorithm. This is made possible by formulating the problem in its most natural (nonlinear) MCP form (namely, in mixed static-kinematic variables) for processing within the GAMS mathematical programming environment. Direct solution of the MCP is made possible by use of the state-of-the-art solver GAMS/PATH. Our algorithm not only reduces significantly the computational effort largely as a result of avoiding the typically burdensome iterative schemes, but also offers increased numerical stability even when large incremental step sizes are used.

The extended limit analysis is formulated as a notoriously difficult to solve instance of a nonconvex and nonsmooth optimization problem, known as an MPEC for which the major source of difficulties is the presence of complementarity conditions. Our proposed algorithm attempts to solve the MPEC as a series of reformulated NLP subproblems for which the complementarity is suitably treated. The penalty NLP-based approach, as confirmed through a large number of numerical tests, can solve robustly and efficiently the underlying MPEC.

We have solved a large number of numerical examples concerning both practical and reasonably sized semirigid frames, four of which are reported in this study. The results all confirm the validity and reliability of our mathematical programming based approaches. From the structural engineering point of view, the results also highlight the influence of semirigid connections, geometric nonlinearity and ductility limitation, namely in typically degrading the maximum load capacity of the structure and softening its post-peak response. We have also confirmed that the adopted stepwise holonomic scheme predicts with sufficient accuracy the actual nonholonomic structural response, and that a simplified 2nd-order geometry assumption is adequate for the class of structures considered.

Finally, we believe that the direct mathematical programming approaches developed can be extended to more sophisticated finite element models and material laws with formal, rather than conceptual, complications.

Acknowledgement

This research was supported by the Australian Research Council through ARC Discovery Grant DP0986332.

Appendix A. 2nd-order geometry and flexible connections

For a generic frame element i in Fig. 4, the two linear compatibility matrix $\mathbf{C}_0^i \in \Re^{3\times 6}$ and associated auxiliary compatibility matrix $\mathbf{C}_f^i \in \Re^{1\times 6}$ read, respectively

$$\mathbf{C}_0^i = \begin{bmatrix} \cos\theta & \sin\theta & 0 & -\cos\theta & -\sin\theta & 0 \\ -\sin\theta/l & \cos\theta/l & 1 & \sin\theta/l & -\cos\theta/l & 0 \\ -\sin\theta/l & \cos\theta/l & 0 & \sin\theta/l & -\cos\theta/l & 1 \end{bmatrix}, \tag{A.1}$$

$$\mathbf{C}_f^i = [-\sin\theta \quad \cos\theta \quad 0 \quad \sin\theta \quad -\cos\theta \quad 0]. \tag{A.2}$$

The effects of both geometric changes and joint semirigidity for an element i with ends a and b (in Fig. 4) are incorporated through the element stiffness matrix $\mathbf{S}^i \in \Re^{3\times 3}$ as follows:

$$\mathbf{S}^i = \begin{bmatrix} EA/l & 0 & 0 \\ 0 & c_1 EI/l & c_2 EI/l \\ 0 & c_2 EI/l & c_3 EI/l \end{bmatrix}, \tag{A.3}$$

where

$$\begin{aligned} c_1 &= \{v_1 k_a k_b + (v_1^2 - v_2^2)k_a\}/k_{ab}, \\ c_2 &= \{v_2 k_a k_b\}/k_{ab}, \\ c_3 &= \{v_1 k_a k_b + (v_1^2 - v_2^2)k_b\}/k_{ab}, \\ k_{ab} &= k_a k_b + v_1(k_a + k_b) + (v_1^2 - v_2^2), \end{aligned}$$

A is the cross-sectional area, I the second moment of area of the central elastic part, E the modulus of elasticity, $k_a = K_0^a l/EI$ (or $k_b = K_0^b l/EI$) a dimensionless stiffness factor with K_0^a (or K_0^b) representing the initial tangent stiffness of the semirigid connection model at end a (or b), see Fig. 2. In the context of 2nd-order geometry (1st-power approximation), the stability functions v_1 and v_2 (Kassimali, 1983) can be appropriately written as

$$v_1 = 4 - \frac{2s_1^i l^2}{15EI}, \tag{A.4}$$

$$v_2 = 2 + \frac{s_1^i l^2}{30EI}. \tag{A.5}$$

Likewise, the elemental matrix $S_f^i \in \Re^{1\times 1}$ reads

$$S_f^i = \frac{-s_1^i}{l}. \tag{A.6}$$

These two matrices are described as functions of the single axial force s_1^i (i.e. $s_1^i > 0$ for compression), and thus the elastic constitution of the geometrically linear case can be recovered by simply assuming a zero member axial force ($s_1^i = 0$). The elastic stiffness matrix $\mathbf{S}^i$ is further modified to accommodate the initial stiffness from a semirigid connection. Obviously, $k_a = 0$ and $k_b = 0$ represent pinned connections (e.g. truss elements). On the other hand, $k_a = \infty$ and $k_b = \infty$ lead to a rigid connection. Intermediate values of k_a and k_b between 0 and ∞ indicate a semirigid connection.

Appendix B. Piecewise linear yield functions

For a generic perfectly plastic ($\mathbf{H}^a = \mathbf{0}$) hinge "$a$" of member i, the piecewise linear (hexagonal) yield condition under combined stresses (Fig. 5a) associated to the nonholonomic relations (8) are

$$\mathbf{w}^{a\mathrm{T}} = [\,w_1 \quad w_2 \quad w_3 \quad w_4 \quad w_5 \quad w_6\,], \tag{B.1}$$

$$\dot{\mathbf{z}}^{a\mathrm{T}} = [\,\dot{z}_1 \quad \dot{z}_2 \quad \dot{z}_3 \quad \dot{z}_4 \quad \dot{z}_5 \quad \dot{z}_6\,],$$

$$\mathbf{s}^{a\mathrm{T}} = [\,s_1^i \quad s_2^i\,],$$

$$\mathbf{N}^a = \begin{bmatrix} 0 & \hat{n} & \hat{n} & 0 & -\hat{n} & -\hat{n} \\ 1 & 1 & -1 & -1 & -1 & 1 \end{bmatrix},$$

$$\mathbf{r}^{a\mathrm{T}} = [\,s_{2u} \quad \tau s_{2u} \quad \tau s_{2u} \quad s_{2u} \quad \tau s_{2u} \quad \tau s_{2u}\,],$$

where $\hat{n} = (s_{2u}/s_{1u})\tan\gamma$ and $\tau = 1 + r_b\tan\gamma$. Yield functions w_1–w_6 govern yielding of hyperplanes 1–6, respectively. When the effect of axial forces on yielding is deemed unnecessary, the pure bending model can be generated by simply retaining only the two functions w_1 and w_4 in (B.1).

The multilinear hardening yield condition (Fig. 5b) accommodates the influence of flexible connections on the inelastic deformation at end "a" of an element i through the corresponding nonholonomic formulations (8) with

$$\mathbf{N}^a = [\,1 \quad -1 \quad 0 \quad 0 \quad 0\,], \quad \mathbf{s}^{a\mathrm{T}} = [s_2^i], \tag{B.2}$$

$$\mathbf{H}^a = \begin{bmatrix} h_1 & h_1 & h_2 - h_1 & h_3 - h_2 & -h_3 \\ h_1 & h_1 & h_2 - h_1 & h_3 - h_2 & -h_3 \\ -h_1 & -h_1 & h_1 & 0 & 0 \\ 0 & 0 & -h_2 & h_2 & 0 \\ 0 & 0 & 0 & -h_3 & h_3 \end{bmatrix},$$

$$\mathbf{w}^a = \begin{bmatrix} w_1 \\ w_2 \\ w_3 \\ w_4 \\ w_5 \end{bmatrix}, \quad \dot{\mathbf{z}}^a = \begin{bmatrix} \dot{z}_1 \\ \dot{z}_2 \\ \dot{z}_3 \\ \dot{z}_4 \\ \dot{z}_5 \end{bmatrix}, \quad \mathbf{r}^a = \begin{bmatrix} M_0 \\ M_0 \\ M_1 - M_0 \\ M_2 - M_1 \\ M_3 - M_2 \end{bmatrix},$$

where the hardening parameters h_j are calculated from

$$h_j = \frac{K_0^a K_j^a}{K_0^a - K_j^a}, \quad \text{for } j = 1, \ldots, 3. \tag{B.3}$$

Obviously, the hardening constitutive law, as given by (B.2), describes the evolution of an isotropic hardening yield model indicating a homothetically expanding yield surface. The assumption of isotropic hardening, it is worth mentioning, is not important for realistic structures under monotonically applied loads since it is unlikely that progressive hardening will activate the opposite yield plane.

In the case of holonomic elastoplastic behavior, the two descriptions (B.1) and (B.2) can be similarly applied to the holonomic relations (11), albeit involving total (rather than rate) quantitative plastic multipliers $\mathbf{z}^a$.

References

Anderson, D., Kavianpour, K., 1991. Analysis of steel frames with semi-rigid connections. Structural Engineering Review 3, 79–87.

Ardito, R., Cocchetti, G., Maier, G., 2008. On structural safety assessment by load factor maximization in piecewise linear plasticity. European Journal of Mechanics – A/Solids 27, 859–881.

Armero, F., Ehrlich, D., 2006. Numerical modeling of softening hinges in thin Euler–Bernoulli beams. Computers and Structures 84, 641–656.

Bird, W.W., Martin, J.B., 1990. Consistent predictors and the solution of the piecewise holonomic incremental problem in elasto-plasticity. Engineering Structures 12, 9–14.

Bolzon, G., Corigliano, A., 1997. A discrete formulation for elastic solids with damaging interfaces. Computer Methods in Applied Mechanics and Engineering 140, 329–359.

Bolzon, G., Tin-Loi, F., 1999. Physical instability and geometric effects in frames. Engineering Structures 21, 557–567.

Brooke, A., Kendrick, D., Meeraus, A., Raman, R., 1998. GAMS: A User's Guide. GAMS Development Corporation, Washington, DC.

Chen, W.F., Zhou, S.P., 1987. Inelastic analysis of steel braced frames with flexible joints. International Journal of Solids and Structures 23, 631–649.

Chen, W.F., 2000. Plasticity, limit analysis and structural design. International Journal of Solids and Structures 37, 81–92.

Cocchetti, G., Maier, G., 2003. Elastic–plastic and limit-state analyses of frames with softening plastic-hinge models by mathematical programming. International Journal of Solids and Structures 40, 7219–7244.

Cottle, R.W., Pang, J.S., Stone, R.E., 1992. The Linear Complementarity Problem. Academic Press, San Diego, CA.

Comi, C., Maier, G., 1990. Extremum theorem and convergence criterion for an iterative solution to the finite-step problem in elastoplasticity with mixed nonlinear hardening. European Journal of Mechanics – A/Solids 9, 563–585.

De Freitas, J.A.T., Lloyd Smith, D., 1984-1985. Elastoplastic analysis of planar structures for large displacements. ASCE Journal of Structural Mechanics 12, 419–445.

Dirkse, S.P., Ferris, M.C., 1995a. MCPLIB: a collection of nonlinear mixed complementarity problems. Optimization Methods and Software 5, 319–345.

Dirkse, S.P., Ferris, M.C., 1995b. PATH solver: a nonmonotone stabilization scheme for mixed complementarity problems. Optimization Methods and Software 5, 123–156.

Drud, A.S., 1994. CONOPT – a large-scale GRG code. ORSA Journal on Computing 6, 207–216.

Ehrlich, D., Armero, F., 2005. Finite element methods for the analysis of softening plastic hinges in beams and frames. Computational Mechanics 35, 237–264.

Ferris, M.C., 1998. MATLAB and GAMS: interfacing optimization and visualization software, Technical Report TR98-19. Computer Sciences Department, University of Wisconsin, Madison, Wisconsin.

Ferris, M.C., Pang, J.S., 1997. Engineering and economic applications of complementarity problems. SIAM Review 39, 669–713.

Ferris, M.C., Tin-Loi, F., 1999. On the solution of a minimum weight elastoplastic problem involving displacement and complementarity constraints. Computer Methods in Applied Mechanics and Engineering 174, 107–120.

Ferris, M.C., Tin-Loi, F., 2001. Limit analysis of frictional block assemblies as a mathematical program with complementarity constraints. International Journal of Mechanical Sciences 43, 209–224.

Forde, B.W.R., Stiemer, S.F., 1987. Improved arc length orthogonality methods for nonlinear finite element analysis. Computers and Structures 27, 625–630.

Franchi, A., Grierson, D.E., Cohn, M.Z., 1981. A computer system for the elastic–plastic analysis of large-scale structures. Mechanics Based Design of Structures and Machines 9, 295–324.

Frye, M.J., Morris, G.A., 1975. Analysis of flexibly connected steel frames. Canadian Journal of Civil Engineering 2, 280–291.

Galea, Y., 1988. Non-linear analysis of plane frame structures with semi-rigid connections. In: Bjorhovde, R. et al. (Eds.), Connections in Steel Structures: Behavior, Strength and Design. Elsevier, London, pp. 222–230.

Kanzow, C., 1996. Some noninterior continuation methods for linear complementarity problems. SIAM Journal on Matrix Analysis and Applications 17, 851–868.

Kassimali, A., 1983. Large deformation analysis of elastic–plastic frames. ASCE Journal of Structural Engineering 109, 1869–1886.

Luo, Z.Q., Pang, J.S., Ralph, D., 1996. Mathematical Programs with Equilibrium Constraints. Cambridge University Press, Cambridge.

Lui, E.M., Chen, W.F., 1988. Behavior of braced and unbraced semi-rigid frames. International Journal of Solids and Structures 24, 893–913.

Maier, G., 1970. A matrix structural theory of piecewise linear elastoplasticity with interacting yield planes. Meccanica 5, 54–66.

Maier, G., 1971. Incremental plastic analysis in the presence of large displacements and physical instabilizing effects. International Journal of Solids and Structures 7, 345–372.

Misa, J.S., 1995. Nonlinear Analysis of Semi-Rigid Frames by Mathematical Programming. Ph.D. Thesis, School of Civil and Environmental Engineering. The University of New South Wales, Sydney.

Przemieniecki, J.S., 1985. Theory of Matrix Structural Analysis. Dover Publication Inc., New York.

Tangaramvong, S., Tin-Loi, F., 2007. A complementarity approach for elastoplastic analysis of strain softening frames under combined bending and axial force. Engineering Structures 29, 742–753.

Tangaramvong, S., Tin-Loi, F., 2009a. Limit analysis of elastoplastic frames considering 2nd-order geometric nonlinearity and displacement constraints. International Journal of Mechanical Sciences 51, 179–191.

Tangaramvong, S., Tin-Loi, F., 2009b. Extended limit analysis of strain softening frames involving 2nd-order geometric nonlinearity and limited ductility. CMES-Computer Modeling in Engineering and Sciences 42, 217–256.

Tangaramvong, S., Tin-Loi, F., 2010a. A constrained non-linear system approach for the solution of an extended limit analysis problem. International Journal for Numerical Methods in Engineering 82, 995–1021.

Tangaramvong, S., Tin-Loi, F., 2010b. The influence of geometric effects on the behavior of strain softening frames. Computational Mechanics 46, 661–678.

Tin-Loi, F., Misa, J.S., 1996. Large displacement elastoplastic analysis of semirigid steel frames. International Journal for Numerical Methods in Engineering 39, 741–762.

Tin-Loi, F., Que, N.S., 2001. Parameter identification of quasibrittle materials as a mathematical program with equilibrium constraints. Computer Methods in Applied Mechanics and Engineering 190, 5819–5836.

Tin-Loi, F., Tangaramvong, S., Xia, S.H., 2007. Limit analysis of frames involving unilateral supports with frictional contact. International Journal of Mechanical Sciences 49, 454–465.